THE EUROPEAN
PHYSICAL JOURNAL C

Nuclear dependence of light neutral meson production in p–A collisions at 400 GeV with NA60

R. Arnaldi[1], K. Banicz[2,3], K. Borer[4], J. Castor[5], B. Chaurand[6], W. Chen[7], C. Cicalò[8], A. Colla[1,9], P. Cortese[9,10], S. Damjanovic[2,3], A. David[2,11], A. De Falco[8,12], A. Devaux[5], L. Ducroux[13], H. En'yo[4], J. Fargeix[5], A. Ferretti[1,9], M. Floris[8,12], A. Förster[2], P. Force[5], N. Guettet[2,5], A. Guichard[13], H. Gulkanian[15], J. M. Heuser[14], P. Jarron[2], M. Keil[2,11], L. Kluberg[6], Z. Li[7], C. Lourenço[2], J. Lozano[11], F. Manso[5], P. Martins[2,11], A. Masoni[8], A. Neves[11], H. Ohnishi[14], C. Oppedisano[1], P. Parracho[2,11], P. Pillot[13], T. Poghosyan[15], G. Puddu[12], E. Radermacher[2], P. Ramalhete[2,11], P. Rosinsky[2], E. Scomparin[1], J. Seixas[11,16,17], S. Serci[8,12], R. Shahoyan[2,11], P. Sonderegger[11], H. J. Specht[3], R. Tieulent[13], A. Uras[8,12,13,a], G. Usai[8,12,b], R. Veenhof[11], H. K. Wöhri[2,11,12], NA60 Collaboration

[1] INFN, Torino, Italy
[2] CERN, Geneva, Switzerland
[3] Physikalisches Institut der Universität Heidelberg, Heidelberg, Germany
[4] University of Bern, Bern, Switzerland
[5] LPC, Université Clermont Auvergne and CNRS-IN2P3, Clermont-Ferrand, France
[6] LLR, Ecole Polytechnique and CNRS-IN2P3, Palaiseau, France
[7] BNL, Upton, NY, USA
[8] INFN, Cagliari, Italy
[9] Università di Torino, Torino, Italy
[10] Università del Piemonte Orientale, Alessandria, Italy
[11] Instituto Superior Tecnico, Dep. Fisica, Lisbon, Portugal
[12] Università di Cagliari, Cagliari, Italy
[13] IPN-Lyon, Univ. Claude Bernard Lyon-I and CNRS-IN2P3, Lyon, France
[14] RIKEN, Wako, Saitama, Japan
[15] YerPhI, Yerevan, Armenia
[16] Center for Physics and Engineering of Advanced Materials (CeFEMA), Lisbon, Portugal
[17] Laboratorio de Intrumentação e Fisica experimental de Particulas (LIP), Lisbon, Portugal

Abstract The NA60 experiment has studied low-mass muon pair production in proton–nucleus collisions with a system of Be, Cu, In, W, Pb and U targets, using a 400 GeV proton beam at the CERN SPS. The transverse momentum spectra of the ρ/ω and ϕ mesons are measured in the full $p_{\rm T}$ range accessible, from $p_{\rm T} = 0$ up to 2 GeV/c. The nuclear dependence of the production cross sections of the η, ω and ϕ mesons has been found to be consistent with the power law $\sigma_{\rm pA} \propto {\rm A}^{\alpha}$, with the α parameter increasing as a function of $p_{\rm T}$ for all the particles, and an approximate hierarchy $\alpha_{\eta} \approx \alpha_{\phi} > \alpha_{\omega}$. The cross section ratios $\sigma_{\eta}/\sigma_{\omega}$, $\sigma_{\rho}/\sigma_{\omega}$ and $\sigma_{\phi}/\sigma_{\omega}$ have been studied as a function of the size A of the production target, and an increase of the η and ϕ yields relative to the ω is observed from p–Be to p–U collisions.

a e-mail: antonio.uras@cern.ch
b e-mail: gianluca.usai@ca.infn.it

1 Introduction

The study of the production of low-mass vector and pseudoscalar mesons in proton–nucleus (p–A) collisions represents a unique tool to understand the role of cold nuclear matter in particle production mechanisms. The nuclear dependence of both the transverse momentum spectra and the total production cross sections is of special interest in this context, with the observations usually interpreted in terms of phenomenological models, since a first-principle description based on non-perturbative QCD is not yet available.

Proton–nucleus collisions have also become of special interest in their own, as a tool to test the possible existence of in-medium modifications of the vector meson spectral functions in cold nuclear matter. The experimental evidence for such effects is at the moment controversial, namely after the KEK-PS E325 [1] and the CLAS [2,3] experiments reporting contradicting observations on possible ρ-meson broadening

and mass-shift in cold nuclear matter. In this context, a recent measurement in p–A collisions at 400 GeV by the NA60 experiment [4], exploiting the same data set considered in the present analysis, ruled out the existence of any significant cold-nuclear matter effect at the SPS energies on the line shapes of the light vector mesons ρ, ω and ϕ, giving in particular, for the first time, a precise characterisation of the ρ-meson line shape in p–A collisions. The aforementioned results from NA60 represent the basis for the new results presented in this letter.

Measurements in p–A collisions also provide a useful cold-nuclear-matter reference for the observations in heavy-ion collisions, allowing for the study of particle production as a function of the size A of the nucleus.

Despite the points of interest mentioned above, there is a general lack of high-precision and high-statistics measurements of low-mass vector and pseudoscalar mesons in proton–nucleus collisions at the SPS energies, in particular for what concerns dilepton data. The nuclear dependence of the production cross sections for π^0, η and ω mesons was investigated at the energy of $\sqrt{s_{NN}} = 29.1$ GeV by the CERES experiment [5] in p–Be and p–Au collisions, and by the HELIOS experiment [6] in p–Be collisions. Results from these experiments were compared to, or complemented the measurements in proton–proton collisions, in particular those performed by the NA27 experiment [7] relative to the production of π^0, η, ω and ρ mesons at $\sqrt{s_{NN}} = 27.5$ GeV. On the other hand, there are no accurate measurements on the nuclear dependence of ϕ production in proton–nucleus collisions at the SPS. At somehow higher energy, $\bar{K}^{*0}$ and ϕ mesons have been recently measured in p-C, p-Ti and p-W interactions at $\sqrt{s_{NN}} = 41.6$ GeV by HERA-B [8].

The NA60 experiment complemented its main In–In programme with a high-luminosity proton–nucleus run, exposing to a 400 GeV proton beam six target materials: Be, Cu, In, W, Pb and U. This allowed for a comprehensive and detailed study of the nuclear dependence of the η, ρ, ω and ϕ meson production. The present letter is organised as follows. First, the p_T spectra are presented for the ρ/ω and ϕ mesons, for which the measurement could be performed down to zero p_T – while the acceptance coverage limited the measurement of η-meson production (via the $\eta \rightarrow \mu\mu\gamma$ Dalitz decay channel) to $p_T > 0.6$ GeV/c. The nuclear dependence of the production cross sections of η, ω and ϕ mesons, integrated over the p_T regions available for each particle, is then investigated in terms of the power law $\sigma_{pA} \propto A^\alpha$. The available statistics also allowed for a dedicated study of the α parameters as a function of p_T. Finally, particle production is further discussed via the study of the cross section ratios in the full phase space, with strangeness enhancement being specifically addressed through the measurement of the nuclear dependence of the cross section ratios $\sigma_\phi/\sigma_\omega$ and $\sigma_\eta/\sigma_\omega$.

2 Apparatus and event selection

During the 2004 run, the NA60 experiment collected data with a system of nine sub-targets of different nuclear species – Be, Cu, In, W, Pb and U – simultaneously exposed to an incident 400 GeV proton beam. The individual target thickness was chosen to have approximately a similar statistical sample from each target. The total interaction length was 7.5%. The beam intensity during the run was 4–5×10^8 protons per second.

A general description of the NA60 apparatus can be found for example in [9], while in [4] some additional, specific details can be found, relevant to the setup used during the proton run of interest for the present analysis.

The produced dimuons are identified and measured by the muon spectrometer, composed of a set of Multi-Wire Proportional Chamber (MWPC) tracking stations, trigger scintillator hodoscopes, a toroidal magnet and a hadron absorber. The material which stops the hadrons also induces multiple scattering and energy loss on the muons, degrading the mass resolution of the measurement made in the spectrometer. To overcome this problem, NA60 already measures the muons before the absorber with a vertex spectrometer, made of pixel silicon detectors. The muon tracks reconstructed in the muon spectrometer are extrapolated back to the target region and matched to the tracks reconstructed in the vertex spectrometer. This is done comparing both their angles and momenta, requiring a *matching* χ^2 less than 3. Once identified, the muons are refitted using the joint information of the muon and the vertex spectrometers. These tracks will be referred to as *matched muons*. Muon pairs of opposite charge are then selected. The matching technique improves significantly the signal-to-background ratio and the dimuon mass resolution. Because of the heavier absorber setup, the mass resolution is slightly worse than during the In–In run: 30–35 MeV/c^2 (depending on target position) at the ω mass (against 23 MeV/c^2 during the In–In run), and the p_T coverage is reduced towards the dimuon mass threshold.

2.1 Target identification

In order to study the nuclear dependence of the yields and the kinematics for the particles produced in the collisions, the identification of the production target is mandatory. In principle, one could consider the origin of the matched dimuon alone, defined as the point of closest approach of its two muon tracks. However, this origin has a limited spatial resolution; in particular, the error associated to the z-position of the dimuon's origin becomes comparable or even larger than the typical semi-distance between targets (5 mm) for masses below 0.45 GeV/c^2. In order to overcome these difficulties, the vertices reconstructed by using all the tracks measured in the silicon telescope (VT vertices) are considered, requiring

that the two muons are attached to the same VT vertex, or to two different VT vertices falling within the same target. The loss of statistics, as studied by Monte Carlo simulations, varies from $\sim 40\%$ for the ϕ mass region, to $\sim 70\%$ in the dimuon mass region below $0.45\,\text{GeV/c}^2$ dominated by the Dalitz decay of the η. After applying this selection, $\sim 80{,}000$ muon pairs are left. The algorithm fails to associate the correct target in $\sim 2\%$ of events at the ϕ mass, $\sim 5\%$ at the ω mass and $\sim 15\%$ in the η Dalitz region: this systematic effect has been studied by means of the same Monte Carlo simulations, and corrected for in the final results.

2.2 Background treatment

The small amount of combinatorial background (originating from π and K decays) is subtracted from the raw dimuon sample: its shape is estimated with an event-mixing technique, while its normalization is established fixing the like-sign (LS) component coming out from the mixing to the LS component of the data (containing no signal from correlated pairs at the SPS energies). In the considered proton–nucleus data, the background accounts for less than 10% of the integrated mass spectrum below $1.4\,\text{GeV/c}^2$. The comparison between mixed and real sample, in turn, gives an average uncertainty of 10% at most, for both the $(++)$ and the $(--)$ components; because of the absolute low level of the background and because of its smooth mass profile, this uncertainty hardly affects the extraction of the signal from the considered dimuon sources.

The background from fake track matches, which could arise at high multiplicities from the association of a muon track to more than one track in the vertex telescope with an acceptable matching χ^2, is significantly lower than the combinatorial background. For this reason, its contribution is almost negligible in the proton–nucleus data – being in any case taken automatically into account by the overlay Monte Carlo technique adopted for the simulations.

3 Monte Carlo simulations, acceptance and reconstruction efficiency

The electromagnetic decays of the light, neutral pseudoscalar and vector mesons (η, η', ρ, ω and ϕ) are the dominating processes at the lower end of the dimuon mass spectrum (from the threshold to the ϕ mass region), adding to the continuum spectrum via their Dalitz decays and/or giving rise to distinct peaks via their 2-body decays. This hadronic decay cocktail was simulated with the NA60 Monte Carlo generator Genesis [10]. The input parameters for the kinematic distributions of the generated processes have been tuned by comparison with the real data, by means of an iterative procedure ensuring self-consistency to the analysis.

The transverse momentum spectra used in the simulations are taken from the analysis itself. The rapidity distributions in the center of mass frame were generated according to the expression $dN/dy \propto 1/\cosh^2(ay)$, similar to a Gaussian of width $\sigma = 0.75/a$, where a describes the empirical functional mass dependence of the width with values of about 0.5 and 0.75 at the masses of $0.14\,\text{GeV/c}^2$ (π^0) and $1\,\text{GeV/c}^2$, respectively [10]. This simple parameterisation has been used by several experiments, since it describes reasonably well existing measurements [11,12].

The muon angular distributions also entering the simulations are assumed to be isotropic for the 2-body decays, while the angular anisotropies of the Dalitz decays, expected to be the same for the pseudo-scalar (η, η') and vector (ω) mesons [13], are described by the distribution:

$$f(\theta) = 1 + \cos^2\theta + \left(\frac{2m_\mu}{M}\right)^2 \sin^2\theta , \qquad (1)$$

where M is the mass of the virtual photon, m_μ the mass of the muon, and θ the angle between the positive muon and the momentum of the parent meson in the rest-frame of the virtual photon [14]. As was explicitly verified, the dimuon acceptance for the Dalitz decays is practically unaffected by the character of the angular distribution, due to the fact that the anisotropy is strongly smeared out in the laboratory frame.

For the mass line shapes of the narrow resonances η, ω and ϕ, a modified relativistic Breit–Wigner parametrization was used, first proposed by Gounaris and Sakurai [15], with widths and masses taken from the Particle Data Group (PDG) tables [16]. For the broad ρ meson the following parameterisation was used [17]:

$$\frac{dN}{dM} \propto \frac{\sqrt{1 - \frac{4m_\mu^2}{M^2}}\left(1 + \frac{2m_\mu^2}{M^2}\right)\left(1 - \frac{4m_\pi^2}{M^2}\right)^{3/2}}{\left(m_\rho^2 - M^2\right)^2 + m_\rho^2\Gamma_\rho^2(M)}$$
$$(MT)^{3/2}\, e^{-\frac{M}{T_\rho}} \qquad (2)$$

with a mass dependent width

$$\Gamma_\rho(M) = \Gamma_{0\rho}\frac{m_\rho}{M}\left(\frac{M^2/4 - m_\mu^2}{m_\rho^2/4 - m_\mu^2}\right)^{3/2}$$
$$= \Gamma_{0\rho}\frac{m_\rho}{M}\left(\frac{q}{q_0}\right)^3 . \qquad (3)$$

The parameters of the ρ parameterisation were either fixed to the PDG values [16], or extracted from the data themselves, as extensively discussed in [4].

The dimuon mass distributions of the η and ω Dalitz decays are described by the QED expectations for point-like particles [18], corrected by the form factors also extracted from the data themselves [4].

The semimuonic simultaneous decays from $D\bar{D}$ mesons produce a smooth open charm continuum with a maximum

at around 1 GeV/c^2. They were simulated with PYTHIA 6.4 [19], with the mass of charm quark set to $m_c = 1.5$ GeV/c^2 and the primordial momentum of the interacting partons generated according to a Gaussian distribution of variance $k_T^2 = 1.0$ (GeV/c)^2.

The Monte Carlo simulations were performed using the overlay technique, which consists of superimposing a Monte-Carlo-generated muon pair onto real events, in order to realistically simulate the underlying hadronic event together with the detector specific behaviour. A real event is read, chosen among the reconstructed data collected by the experiment, containing a high-mass matched dimuon (within the J/ψ mass window, the two stiff muons guaranteeing an unambiguous identification of the interaction target) whose vertex is imposed to be the origin of the generated muon pair. Alternatively, dimuons whose vertex has the z-coordinate determined with an uncertainty smaller than 3 mm were also used. This second choice, applying weaker conditions on the vertex candidates, has been considered for systematic checks in the analysis. The muon pair produced in the simulation is tracked through the NA60 apparatus, using GEANT3 [20]. Starting from the ensemble of simulated and real hits, the events in which a muon pair gave rise to a trigger were reconstructed using the same reconstruction settings used for the real data. To make the MC simulation as realistic as possible, the MC tracks leave a signal in a given pixel plane with a probability proportional to the plane efficiency as estimated from the analysis of the real data.

The p_T dependence of the dimuon acceptance results from a complex convolution of several factors: the geometric acceptance of the vertex telescope, the energy loss of muons in the hadron absorber, the geometric requirements embedded in the trigger logic of the muon spectrometer (which requires two muons to belong to different sextants), the combination of the magnetic fields provided by the dipole magnet in the vertex region and the toroidal magnet in the muon spectrometer after the absorber. An additional loss of factor up to ∼ 2 is caused by the reconstruction efficiency. In Fig. 1 the dimuon acceptance × reconstruction efficiency as a function of p_T is shown for the three processes $\eta \to \mu^+\mu^-\gamma$, $\omega \to \mu^+\mu^-$ and $\phi \to \mu^+\mu^-$, on which the extraction of the η, ω and ϕ yields is based. For each process, the p_T dependence is shown for the Uranium, Indium and Lead targets, respectively sitting in the initial, central and final part of the target system. In the 2004 p–A run the acceptance was lower than during the In–In run. This was due to a combination of several factors, the most important being the replacement of 40 cm of graphite with 40 cm of iron in the final part of the hadron absorber. Other factors contributing to the loss of acceptance were the reduced tracking efficiencies both for the muon spectrometer (due to 5 MWPC broken planes) and the vertex spectrometer (one tracking plane permanently switched off and the others having much reduced efficiencies

with respect to the In–In run, because of ageing effects), as well as the selections imposed in the analysis for the identification of the production target.

4 Signal extraction

The signal extraction for the dimuon sources of interest for the present analysis is based on a fit of the dimuon mass spectrum, after the subtraction of the combinatorial background. In the fit procedure, the data points are compared to the superposition of the expected MC sources in the mass region from the threshold up to 1.4 GeV/c^2, as explained in [4].

Any possible ρ/ω interference effect is neglected in the fits performed in the present analysis, as justified by the results discussed in [4]. The contribution of the Dalitz decay $\eta' \to \mu^+\mu^-\gamma$ accounts for a very small fraction of the total dimuon yield; for this reason, and because of its continuum shape having no dominant structure apart from the broad peak at the ρ mass (due to the contribution of the ρ to the η' form factor), the fit to the reconstructed mass spectrum is not sensitive to this contribution, and the ratio $\sigma_{\eta'}/\sigma_\omega$ was fixed to 0.12 [10,21]. The relative branching ratios $BR(\eta \to \mu\mu)/BR(\eta \to \mu\mu\gamma)$ and $BR(\omega \to \mu\mu\pi^0)/BR(\omega \to \mu\mu)$ have been fixed to the PDG value [16] and to the value obtained from the analysis of the target-integrated mass spectrum [4], respectively. The normalisation of the ρ-meson 2-body decay has been left free in the p_T-integrated fits, where the available data samples were large enough to allow for a robust extraction of the corresponding signal; it was otherwise fixed to $\sigma_\rho/\sigma_\omega = 1$, as justified by the p_T-integrated results. All the other processes have their normalisations free.

The evaluation of the systematics on the signal extraction is performed by repeating the fits on the dimuon mass spectra, each time varying the following parameters of the input configuration: (1) the cross section ratio $\sigma_{\eta'}/\sigma_\omega$ was varied by $\pm 50\%$ with respect to the nominal value 0.12; (2) the combinatorial background normalisation was varied by $\pm 20\%$; (3) the ratio $\sigma_\rho/\sigma_\omega$, when fixed, was varied by $\pm 10\%$ around the nominal value $\sigma_\rho/\sigma_\omega = 1$; (4) the relative branching ratios between the 2-body and Dalitz decays of the η and ω mesons were varied by the uncertainties associated to the existing measurements [4,16]; (5) the cut on the matching χ^2 for the single muons was varied in the interval 2–3; (6) two settings for the choice of the production vertices in the overlay MC were used, as described in the previous section.

A possible bias in the estimation of the open charm contribution has also been considered, due to the fact that the Drell-Yan process, which does not give any appreciable contribution below 1 GeV/c^2 while contributing above, is neglected in the fits. In order to study the corresponding systematic effect, each fit has been repeated scaling the open charm pro-
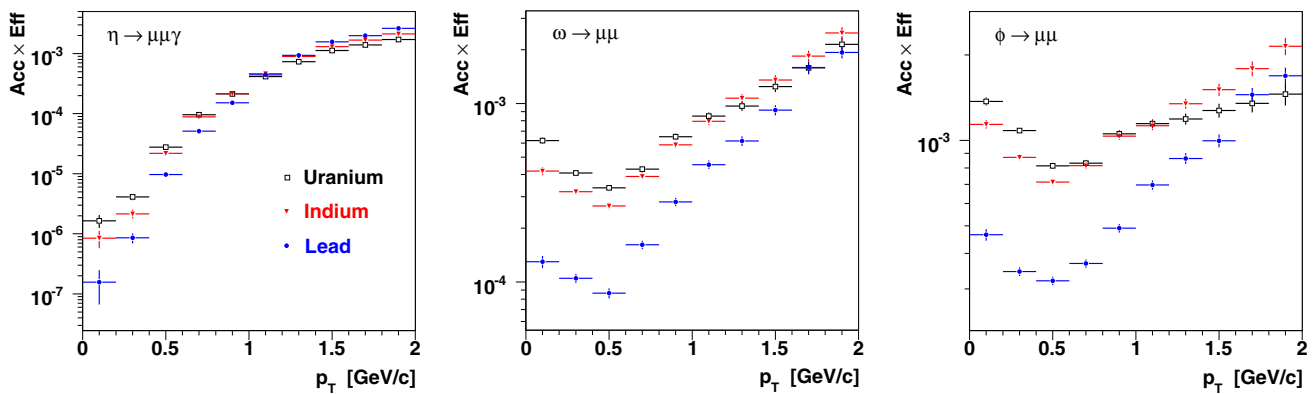
Fig. 1 Acceptance × reconstruction efficiency vs p_T for the Uranium, Indium and Lead targets, for the three processes $\eta \to \mu^+\mu^-\gamma$, $\omega \to \mu^+\mu^-$ and $\phi \to \mu^+\mu^-$

cess down to 80% and 60% of the level optimised by the fit when the contribution is left free.

5 p_T spectra of the ρ/ω and ϕ mesons

In this section we present the analysis of the transverse momentum spectra for the ρ/ω and ϕ mesons. To build the raw p_T spectra we start by dividing the real data sample, target by target, into p_T intervals of 200 MeV/c, sufficiently larger than the p_T resolution of the apparatus in order for residual smearing effects to be safely neglected. The same selection is then applied to the MC spectra for all the signal sources, as well as to the contribution accounting for the combinatorial background. The available statistics is significant up to $p_T \sim 2$ GeV/c. For each target and p_T interval, a fit is then performed on the dimuon mass spectrum after the subtraction of the combinatorial background. In this way, the contributions coming from the 2-body decays of the ω and ϕ mesons can be evaluated, and a raw p_T spectrum is extracted for each particle. This is then corrected for the acceptance × efficiency as a function of p_T, estimated through the MC simulations. For sufficiently narrow p_T bins, this correction is independent of the p_T function used as input for the MC simulations.

Dividing the total sample into several p_T intervals strongly reduces the statistics available for each mass spectrum fit, making it impossible to properly disentangle the ρ contribution under the ω peak. For this reason, the constraint $\sigma_\rho/\sigma_\omega = 1$ is imposed in these fits, as justified by the p_T-integrated analysis of the production cross section ratios as a function of the target size A, discussed in the last section. Whenever the $\sigma_\rho/\sigma_\omega = 1$ constraint is imposed in the analysis, the results are referred to ρ/ω instead of ρ or ω separately.

The ρ/ω and ϕ p_T spectra resulting after the correction for the acceptance × efficiency are shown in Figs. 2 and 3 as a function of the transverse mass m_T and p_T^2. The m_T spectra have been compared to the thermal-like function:

$$\frac{1}{p_T}\frac{dN}{dp_T} = \frac{1}{m_T}\frac{dN}{dm_T} = 2\frac{dN}{dp_T^2} \propto \exp\left(-\frac{m_T}{T}\right). \tag{4}$$

One can immediately appreciate how the thermal hypothesis clearly fails in describing the spectra in the whole available kinematic range, showing a systematic deviation from the pure exponential trend. The fact that such a deviation was not observed in peripheral In–In collisions at 158 AGeV [22], resulting in a hardening of the spectra reported in the present analysis, could be attributed to the larger collision energy in the p–A data.

The fit with the exponential function has thus been limited to $(m_T - m_0) < 0.8$ GeV/c^2 and $(m_T - m_0) < 0.7$ GeV/c^2 for the ρ/ω and the ϕ mesons, respectively, where the thermal hypothesis is found to describe the data reasonably well (solid, red line); the extrapolation of the resulting fit function up to the upper end of the available m_T range is shown as a dashed, blue line, helping to appreciate the contribution of the hard tail at high p_T. The T values found from the fits are compiled in Table 1, where both statistical and systematic uncertainties are reported, the latter reflecting squared sum of the systematic uncertainty on the signal extraction, discussed in the previous section. When evaluating the systematic uncertainty on the T parameter, the upper limit of the fit range was also changed by the m_T quantity equivalent to 200 MeV/c in p_T, since the limit of the range where the thermal-like part of the distribution dominates over the hard tail cannot be precisely established.

The superposition of a thermal-like distribution at low p_T and a hard tail at high p_T, favored by the data, can be modeled by means of the following power-law function, used for example by the HERA-B Collaboration to describe the p_T^2 spectrum of the ϕ meson [8]:

$$\frac{dN}{dp_T^2} \propto \left(1 + \frac{p_T^2}{p_0^2}\right)^{-\beta}, \tag{5}$$

a standard form where the $(1+\ldots)$ term dominates in the limit of vanishing p_T, and the $p_T^{-\beta}$ dependence is characteristic of

hard processes. The fits based on this power-law function successfully extend up to the upper end of the available p_T^2 range, as it can be appreciated from the right panels of Figs. 2 and 3. The β and p_0^2 parameters are listed in Table 1 with their statistical and systematic uncertainties, the latter reflecting the squared sum of the systematic uncertainties on the signal extraction, discussed in the previous section.

No significant trend for the p_0^2 or β parameters, as a function of the production target, can be inferred from the fit results within the statistical and systematic uncertainties. To get more insight into this aspect, in Table 1 we also compile the mean value of p_T for each target, as extracted from the corresponding power-law fit function. The errors associated to each value of $\langle p_T \rangle$ reflect the statistical and systematic uncertainties on the p_0^2 or β parameters. No definite trend as a function of the target can be identified here, too. To compare the ρ/ω and ϕ p_T spectra, then, the target-integrated values are considered – profiting from a better statistical accuracy. One finds $\langle p_T \rangle_{\rho/\omega}^{\mathrm{NA60, \, p-A}} = 0.61 \pm 0.03$ (stat.) $\pm$ 0.03 (syst.) GeV/c, $\langle p_T \rangle_{\phi}^{\mathrm{NA60, \, p-A}} = 0.70 \pm 0.04$ (stat.) $\pm$ 0.02 (syst.) GeV/c.

The results obtained for the p_T spectra of the ρ/ω and ϕ mesons can be compared to the available experimental results. The NA27 Collaboration measured the η, ρ, ω and ϕ production in p–p collisions at $\sqrt{s} = 27.5$ GeV [7]. No data point is shown by the NA27 Collaboration for the p_T spectra of the ω and ϕ mesons, for which only the fit results are given, relative to the function $dN/dp_T^2 \propto \exp(-\delta p_T^2)$, with the quoted values for the δ parameter being: $\delta_\omega = 2.25 \pm 0.16$ (GeV/c)$^{-2}$, $\delta_\phi = 2.98 \pm 0.35$ (GeV/c)$^{-2}$. From these parameters one finds $\langle p_T \rangle_\omega^{\mathrm{NA27}} = (0.591 \pm 0.021)$ GeV/c and $\langle p_T \rangle_\phi^{\mathrm{NA27}} = (0.513 \pm 0.030)$ GeV/c. As one can see, the $\langle p_T \rangle$ for the ω meson extracted from the fit function of NA27 agrees with the estimate obtained in the present analysis, while for the $\langle p_T \rangle$ of the ϕ meson a difference of more than 4 (statistical) standard deviations is found. Furthermore, the present NA60 results clearly indicate that $\langle p_T \rangle_\phi > \langle p_T \rangle_{\rho/\omega}$, while the NA27 results imply that $\langle p_T \rangle_\phi < \langle p_T \rangle_\omega$.

Concerning the p_T measurement for the ϕ-meson, the present results can be also compared to the ones obtained by the HERA-B Collaboration [8], which measured ϕ-meson production (in the K^+K^- channel) in p-C, p-Ti and p-W collisions at $\sqrt{s_{NN}} = 41.6$ GeV. Keeping in mind the different energies between the NA60 and the HERA-B data, the p_T distributions are well described in both cases by the power-law function (5). As in the present analysis, no definite trend for the $\langle p_T \rangle$ as a function of the target is found by HERA-B. The p_0^2, β parameters and the mean p_T measured by HERA-B are compatible with the NA60 measurements shown in Table 1; in particular, for the Tungsten target

common to both the NA60 and HERA-B data, the following values are found: $p_0^2(\mathrm{HERA\text{-}B}) = 1.65 \pm 0.14$ (GeV/c)^2, $\beta(\mathrm{HERA\text{-}B}) = 4.20 \pm 0.14$, $\langle p_T \rangle_\phi^{\mathrm{HERA\text{-}B, \, p\text{-}W}} = (0.72 \pm 0.09)$ GeV/c, to be compared to the NA60 results listed in Table 1.

## 6 Nuclear dependence of the η, ω and ϕ production cross sections

6.1 p_T-integrated analysis

The p_T-integrated yields of the η, ω and ϕ mesons are extracted from the fits shown in Fig. 4. As one can see, the comparison between the sum of the MC sources and the dimuon mass spectrum is satisfactory over the whole mass range for each target. The yields are then corrected for the acceptance $\times$ efficiency evaluated in the full phase space, and normalised to the number of nuclear interaction lengths of each target. The small beam attenuation seen by the downstream targets is also taken into account and corrected for. In the case of the η-meson, the difference between the kinematics of the parent meson and the dimuon has been properly estimated by means of a MC simulation of the Dalitz process, and the results properly corrected for.

In the following, the nuclear dependence of the production cross-sections, normalised to the lightest target is presented. The absolute cross-sections could not be determined because of a malfunctioning of the argonium counter devoted the beam luminosity measurement. The relative production cross sections for the ω, ϕ and η mesons, normalised to the Beryllium target, are shown in the left panels of Fig. 5. The cross section for the ρ-meson was found to be compatible with the one of the ω-meson within the errors, independent of the target, and is not shown here (see Sect. 7). The nuclear dependence of the production cross sections has been parameterised with the power law $\sigma_{pA} \propto A^\alpha$ [23]: the fit functions are shown as solid, red lines in Fig. 5, giving $\alpha_\omega = 0.841 \pm 0.014$ (stat.) ± 0.030 (syst.), $\alpha_\phi = 0.906 \pm 0.011$ (stat.) ± 0.025 (syst.) and $\alpha_\eta = 0.935 \pm 0.048$ (stat.) ± 0.060 (syst.).

Fixing the reference for the relative cross sections to the Beryllium nucleus could induce a bias in the analysis of the nuclear dependence of particle production. Accounting for 9 nucleons only, indeed, the Be nucleus could behave more as an incoherent superposition of single nucleons rather than as a nuclear system having collective properties – as in the case of the heavier nuclei. This could lead to a breaking of the power-law dependence $\sigma_{pA} \propto A^\alpha$ for the Be target, biasing the extraction of the α parameters. For this reason, the option to normalise the production cross sections to the Cu target, excluding the Be point from the fit, was also considered as

Fig. 2 Left: fits on the acceptance-corrected m_T spectra of the ρ/ω mesons, with the exponential function (4). Right: Fits on the acceptance-corrected p_T^2 spectra of the ρ/ω mesons, with the power-law (5)
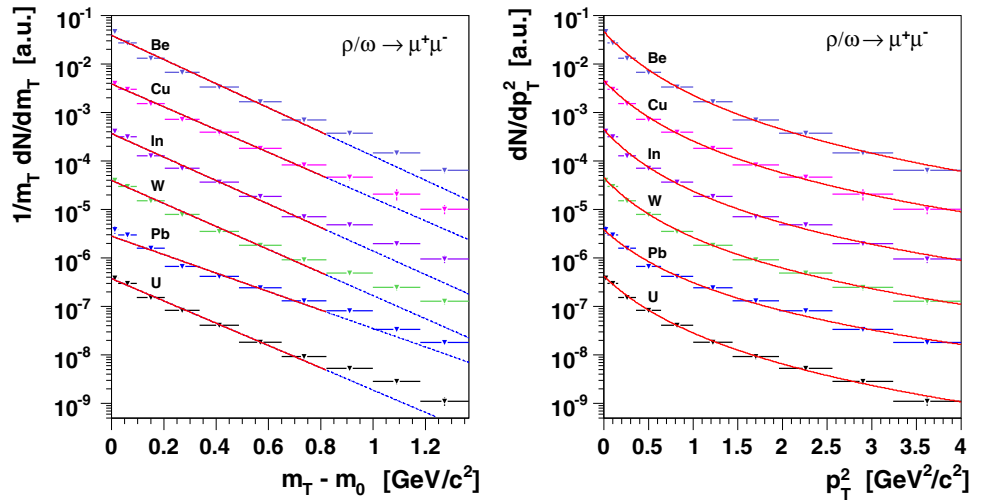

Fig. 3 Left: Fits on the acceptance-corrected m_T spectra of the ϕ meson, with the exponential function (4). Right: Fits on the acceptance-corrected p_T^2 spectra of the ϕ meson, with the power-law (5)
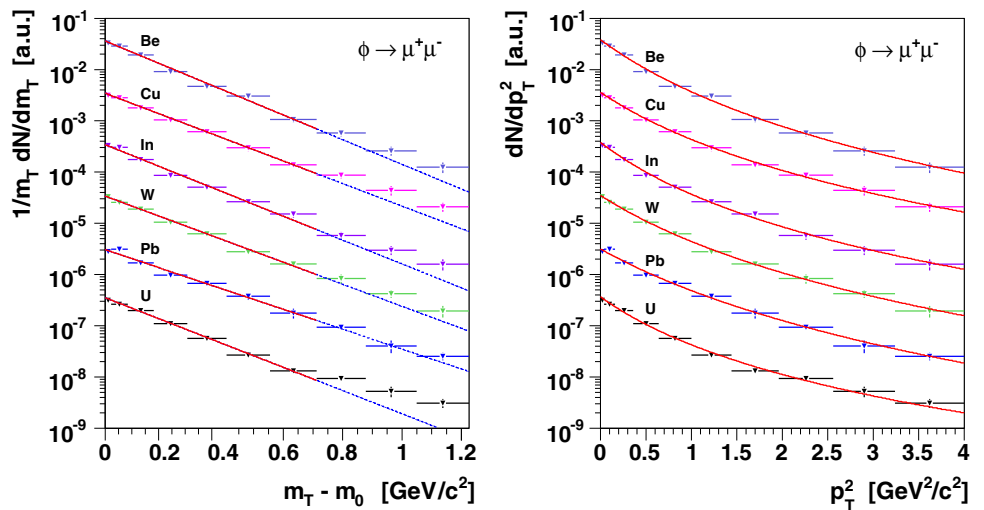
Table 1 Results for the ρ/ω and ϕ transverse momentum spectra as a function of A: T-values as obtained from thermal functions; p_0^2, β and $\langle p_T \rangle$ as obtained from the power-law fit functions

Target		T [MeV]	p_0^2 [GeV^2/c^2]	β	$\langle p_T \rangle$ [GeV/c]
ρ/ω	Be	$179 \pm 4 \pm 7$	$0.98 \pm 0.11 \pm 0.13$	$4.07 \pm 0.24 \pm 0.27$	$0.57 \pm 0.04 \pm 0.05$
	Cu	$185 \pm 4 \pm 10$	$0.79 \pm 0.10 \pm 0.12$	$3.45 \pm 0.22 \pm 0.24$	$0.60 \pm 0.05 \pm 0.06$
	In	$184 \pm 4 \pm 7$	$0.69 \pm 0.09 \pm 0.08$	$3.27 \pm 0.20 \pm 0.15$	$0.62 \pm 0.05 \pm 0.03$
	W	$185 \pm 4 \pm 11$	$0.66 \pm 0.07 \pm 0.02$	$3.08 \pm 0.16 \pm 0.12$	$0.62 \pm 0.05 \pm 0.03$
	Pb	$223 \pm 10 \pm 22$	$0.74 \pm 0.14 \pm 0.08$	$2.94 \pm 0.24 \pm 0.17$	$0.69 \pm 0.10 \pm 0.06$
	U	$188 \pm 4 \pm 10$	$0.82 \pm 0.10 \pm 0.10$	$3.40 \pm 0.21 \pm 0.23$	$0.62 \pm 0.05 \pm 0.06$
	ALL	$188 \pm 2 \pm 9$	$0.76 \pm 0.03 \pm 0.05$	$3.31 \pm 0.07 \pm 0.13$	$0.61 \pm 0.03 \pm 0.03$
ϕ	Be	$183 \pm 6 \pm 6$	$1.83 \pm 0.42 \pm 0.23$	$5.27 \pm 0.83 \pm 0.46$	$0.64 \pm 0.11 \pm 0.06$
	Cu	$198 \pm 6 \pm 6$	$1.50 \pm 0.31 \pm 0.09$	$4.13 \pm 0.55 \pm 0.16$	$0.70 \pm 0.11 \pm 0.03$
	In	$188 \pm 6 \pm 13$	$1.21 \pm 0.22 \pm 0.10$	$3.90 \pm 0.43 \pm 0.22$	$0.66 \pm 0.09 \pm 0.04$
	W	$202 \pm 6 \pm 5$	$1.73 \pm 0.33 \pm 0.08$	$4.50 \pm 0.56 \pm 0.19$	$0.70 \pm 0.10 \pm 0.03$
	Pb	$222 \pm 9 \pm 16$	$2.11 \pm 0.58 \pm 0.43$	$4.90 \pm 0.90 \pm 0.61$	$0.72 \pm 0.15 \pm 0.10$
	U	$192 \pm 5 \pm 1$	$1.14 \pm 0.21 \pm 0.19$	$3.44 \pm 0.39 \pm 0.41$	$0.73 \pm 0.11 \pm 0.11$
	ALL	$193 \pm 2 \pm 5$	$1.27 \pm 0.10 \pm 0.07$	$3.81 \pm 0.17 \pm 0.07$	$0.70 \pm 0.04 \pm 0.02$

Fig. 4 Fits on the p_T-integrated dimuon mass spectra for the different production targets, with the superposition of the expected sources: $\eta \to \mu^+\mu^-\gamma$ (light green, dominating for masses below 0.5 GeV/c^2), $\eta \to \mu^+\mu^-$ (magenta), $\rho \to \mu^+\mu^-$ (cyan), $\omega \to \mu^+\mu^-\pi^0$ (blue), $\omega \to \mu^+\mu^-$ (dark green), $\eta' \to \mu^+\mu^-\gamma$ (yellow), $\phi \to \mu^+\mu^-$ (dark violet), and the open charm process (grey)
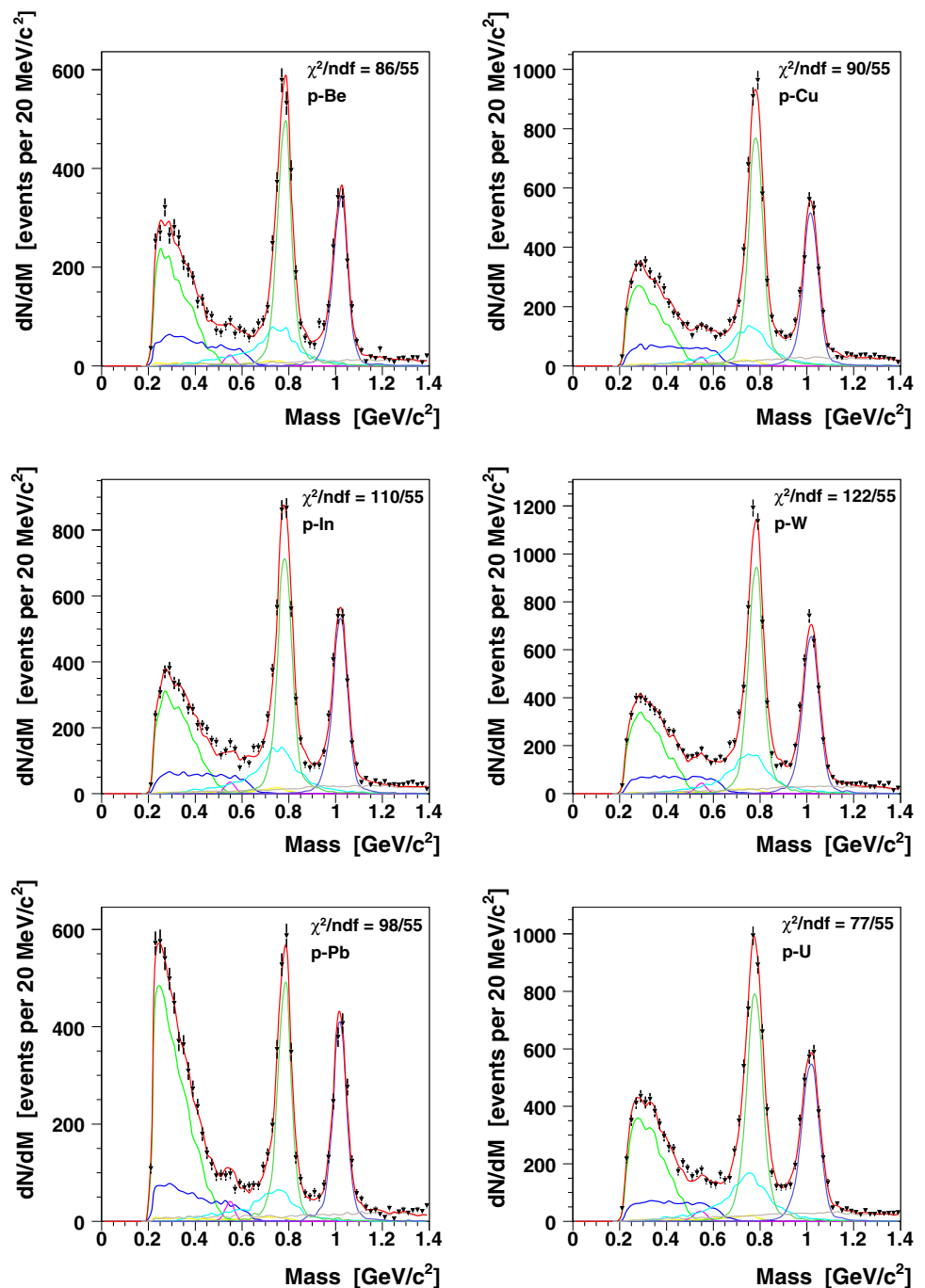
a cross-check: the corresponding results on the α parameters, affected by larger statistical uncertainties because of the much reduced lever arm, and not shown here, were found to be compatible within the uncertainties to the ones presented above.

6.2 p_T-differential analysis

The p_T-dependence of the α parameters for the η, ω and ϕ mesons has also been studied, considering p_T intervals of 200 MeV/c and starting from $p_T = 0$ for the ω and ϕ mesons and from $p_T = 0.6$ GeV/c for the η meson. For each slice of p_T, the α_η, α_ω and α_ϕ parameters have been extracted, together with their statistical and systematic uncertainties, by applying the same procedure discussed in the previous section for the p_T-integrated measurement. The α parameters are shown in Table 2 and their p_T dependence is summarised on the right column of Fig. 5: in each plot, the error bars and the shadowed boxes account for the statistical and systematic uncertainties, respectively. It was also verified (not shown

Fig. 5 Left column: fit on the relative production cross sections for the ω, ϕ and η mesons as a function of A, normalized to the Be or the Cu target. Right column: p_T dependence of the α parameter for the ω, ϕ and η mesons
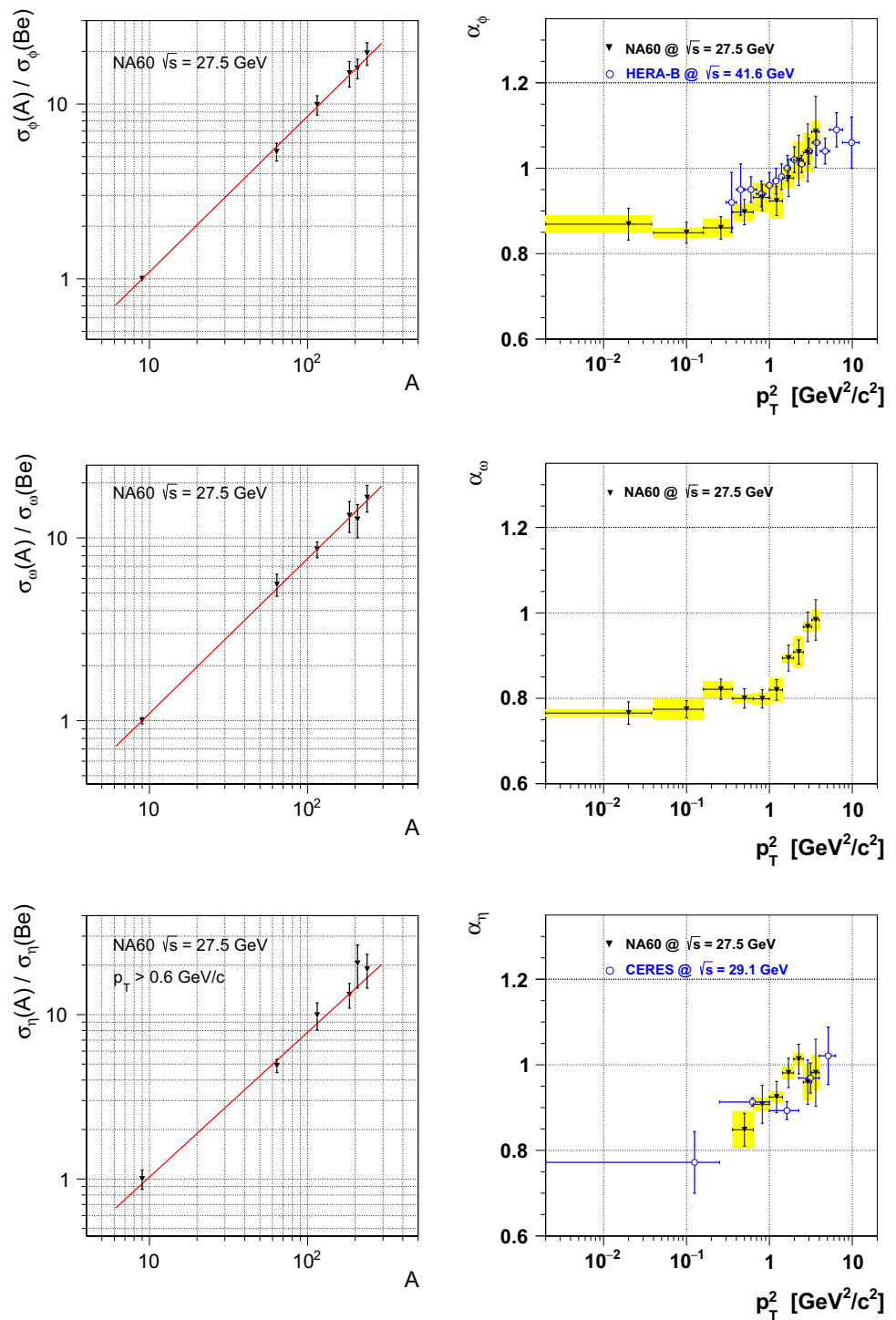
here) that the same trend of the α parameters as a function of p_T, although with significantly larger uncertainties, could be found when excluding the Be target from the analysis, setting the relative normalisation to the Cu target.

The α parameters increase as a function of p_T for the three considered particles, a behaviour which can be related to the so-called "Cronin effect" originally observed by Cronin *et*

al. for charged kaons [24]. The trend of the α parameters can also be interpreted as a consequence of the hardening of the particle production mechanism with p_T, with values of α closer to the "black disk" limit $\alpha = 2/3$ for $p_T \approx 0$, as expected for soft production mechanisms scaling with the surface of the target nucleus, and values closer to the $\alpha = 1$ limit for $p_T \gtrsim 1.5$ GeV/c, as expected for hard production

Table 2 Results for the α parameter as a function of p_T for the η, ω and ϕ mesons

Δp_T [GeV/c]	α_η	α_ω	α_ϕ
$0.0 - 0.2$	–	$0.77 \pm 0.03 \pm 0.01$	$0.87 \pm 0.04 \pm 0.02$
$0.2 - 0.4$	–	$0.77 \pm 0.02 \pm 0.02$	$0.85 \pm 0.02 \pm 0.01$
$0.4 - 0.6$	–	$0.82 \pm 0.02 \pm 0.02$	$0.86 \pm 0.03 \pm 0.02$
$0.6 - 0.8$	$0.85 \pm 0.04 \pm 0.04$	$0.80 \pm 0.02 \pm 0.01$	$0.90 \pm 0.03 \pm 0.02$
$0.8 - 1.0$	$0.91 \pm 0.04 \pm 0.02$	$0.80 \pm 0.02 \pm 0.02$	$0.93 \pm 0.03 \pm 0.03$
$1.0 - 1.2$	$0.92 \pm 0.04 \pm 0.02$	$0.82 \pm 0.02 \pm 0.03$	$0.92 \pm 0.03 \pm 0.04$
$1.2 - 1.4$	$0.98 \pm 0.03 \pm 0.02$	$0.89 \pm 0.03 \pm 0.01$	$0.98 \pm 0.04 \pm 0.02$
$1.4 - 1.6$	$1.01 \pm 0.04 \pm 0.02$	$0.91 \pm 0.03 \pm 0.04$	$1.02 \pm 0.06 \pm 0.04$
$1.6 - 1.8$	$0.96 \pm 0.05 \pm 0.04$	$0.97 \pm 0.03 \pm 0.01$	$1.04 \pm 0.07 \pm 0.04$
$1.8 - 2.0$	$0.98 \pm 0.08 \pm 0.04$	$0.98 \pm 0.05 \pm 0.02$	$1.09 \pm 0.08 \pm 0.02$

mechanisms scaling with the number of available nucleons. An additional hardening of the production mechanism could be attributed to the $s\bar{s}$ component in the quark wave function of the measured hadrons: in absence of explicit theoretical calculations for the α parameters, this simple assumption could still qualitatively explain the larger values measured for α_ϕ and α_η, with respect to α_ω.

The nuclear dependence of the production cross sections for the light neutral mesons has been studied by previous experiments for the ϕ meson, although at energy regimes often different from the one considered in the present analysis. The α parameter for the ϕ meson has been measured by the NA11 Collaboration, at the CERN-SPS, studying collisions of 120 GeV protons on beryllium and tantalum targets, in the $\phi \to K^+K^-$ decay channel [25]. They obtained a value $\alpha_\phi = 0.86 \pm 0.02$ (with a systematic uncertainty estimated to be around three times smaller than the statistical one) for ϕ mesons produced in the phase space window $0 < x_F < 0.3$ and $p_T < 1$ GeV/c. The BIS-2 Collaboration, at Serpukhov, measured the α value of the ϕ mesons produced in collisions induced by neutrons of energies between 30 and 70 GeV colliding on carbon, aluminum and copper targets, considering the $\phi \to K^+K^-$ decay channel [26], obtaining $\alpha_\phi = 0.81 \pm 0.06$ for ϕ mesons produced with $x_F > 0$ and $p_T < 1$ GeV/c (without mentioning systematic errors). More recently, as already mentioned in the the analysis of the p_T spectra, the HERA-B experiment at DESY studied ϕ-meson production in p-C, p-Ti and p-W collisions at $\sqrt{s_{NN}} = 41.6$ GeV [8]. HERA-B found a value $\alpha_\phi = 0.96 \pm 0.02$ in the phase space covered by the detector, $-0.7 < y_{cms} < 0.25$ and $0.3 < p_T^2 < 12$ (GeV/c)^2. Extrapolating the measurements to zero p_T, the value for α_ϕ decreases to $\alpha_\phi = 0.91 \pm 0.02$ (where the error includes the systematic uncertainty). The HERA-B results also suggest an increase of the α_ϕ parameter with p_T (also reported for the K^{*0} and for the $\bar{K}^{*0}$ mesons), with values of α_ϕ as large as 1.1 for $p_T^2 \sim 10$ (GeV/c)^2. A remarkable agreement is observed between the p_T-dependence of α_ϕ measured in the present

analysis and the results of HERA-B, as shown in the right-top panel of Fig. 5. The KEK-PS E325 experiment [1] also measured the α parameter for the ϕ meson, studying its e^+e^- decay in p-C and p-Cu collisions at $\sqrt{s_{NN}} = 5.1$ GeV. In the region of $0.9 < y < 1.7$ and $p_T < 0.75$ GeV/c they found $\alpha_\phi = 0.937 \pm 0.049 \pm 0.018$, larger than the NA60 measurement in the same p_T range, but still compatible within the uncertainties. Summarising, despite the different collision systems, energies and also kinematic regions, there is a substantial agreement between the α_ϕ value extracted from the present analysis and the values from previous measurements.

A comparison of the results on the α_η parameter can be established with the data published by the CERES-TAPS Collaboration [5]: good agreement is observed between the two sets of data points, as shown in the right-bottom panel of Fig. 5. No similar comparison is possible for the ω, due to the lack of available measurements. The only available value for the ω meson is reported by the KEK-PS E325 Collaboration, already cited for the ϕ meson, which measured $\alpha_\omega = 0.710 \pm 0.021 \pm 0.037$, compatible with the value of α for the total inelastic p–A cross section and somehow smaller than our result.

7 Particle cross-section ratios in full phase space

We finally consider the nuclear dependence of the particle cross-section ratios in full phase space, assuming the ω meson as the reference. The results are compiled in Table 3.

The $\sigma_\rho/\sigma_\omega$ ratio – shown in the left panel of Fig. 6 – appears to be flat with A. The ratio averaged over the different targets, indicated by a horizontal line, is $\sigma_\rho/\sigma_\omega = 1.00 \pm 0.04$ (stat.) ± 0.04 (syst.), in agreement with the ratio $\rho/\omega = 0.98 \pm 0.08$ measured in p–p collisions at $\sqrt{s} = 27.5$ GeV by the NA27 experiment [7], also shown in the figure.

The $\sigma_\phi/\sigma_\omega$ ratio is shown in the right panel of Fig. 6. The trend of the NA60 data points points to a ~ 20 % increase of

Table 3 Results for the cross section ratios $\sigma_\eta/\sigma_\omega$, $\sigma_\rho/\sigma_\omega$ and $\sigma_\phi/\sigma_\omega$ as a function of the production target

A	$\sigma_\eta/\sigma_\omega$	$\sigma_\rho/\sigma_\omega$	$\sigma_\phi/\sigma_\omega$
Be	$1.42 \pm 0.08 \pm 0.17$	$0.94 \pm 0.10 \pm 0.09$	$0.086 \pm 0.004 \pm 0.003$
Cu	$1.51 \pm 0.07 \pm 0.16$	$0.91 \pm 0.08 \pm 0.07$	$0.083 \pm 0.004 \pm 0.003$
In	$1.89 \pm 0.09 \pm 0.21$	$1.17 \pm 0.10 \pm 0.09$	$0.097 \pm 0.004 \pm 0.003$
W	$1.87 \pm 0.08 \pm 0.25$	$0.97 \pm 0.08 \pm 0.14$	$0.097 \pm 0.004 \pm 0.003$
Pb	$2.34 \pm 0.12 \pm 0.20$	$0.95 \pm 0.02 \pm 0.11$	$0.108 \pm 0.006 \pm 0.003$
U	$2.04 \pm 0.09 \pm 0.27$	$1.08 \pm 0.09 \pm 0.11$	$0.100 \pm 0.004 \pm 0.004$

Fig. 6 Left: production cross section ratio $\sigma_\rho/\sigma_\omega$ as a function of A. Right: $\sigma_\phi/\sigma_\omega$ as a function of A. The ratios refer to the full phase space, the error bars and shadowed boxes account for statistical and systematic uncertainties, respectively
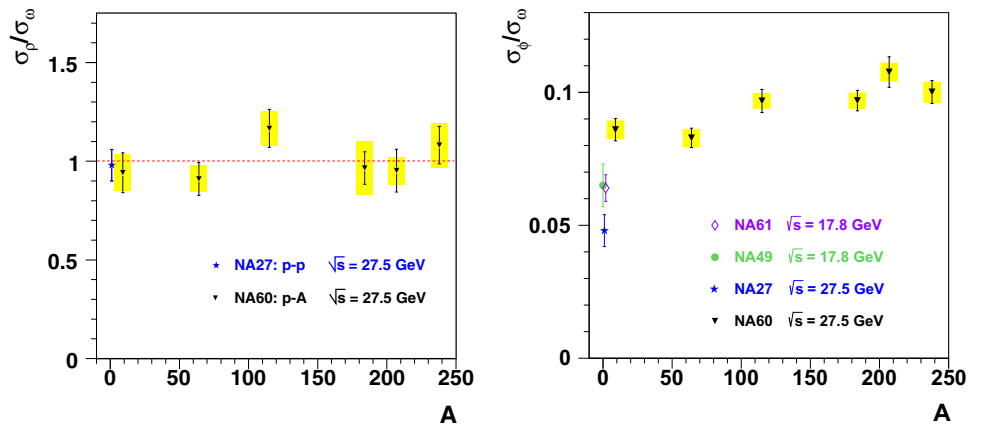
Fig. 7 Left: compilation of the available p_T measurements for the η and fit with the power-law function (5). Right: cross section ratio $\sigma_\eta/\sigma_\omega$ as a function of A. The ratios refer to the full phase space, the error bars and shadowed boxes account for statistical and systematic uncertainties, respectively. An additional 10 % systematics uncertainty common to the NA60 points, coming from the uncertainty on the extrapolation factor to full phase space of the η measurement, is represented by the band on the vertical axis
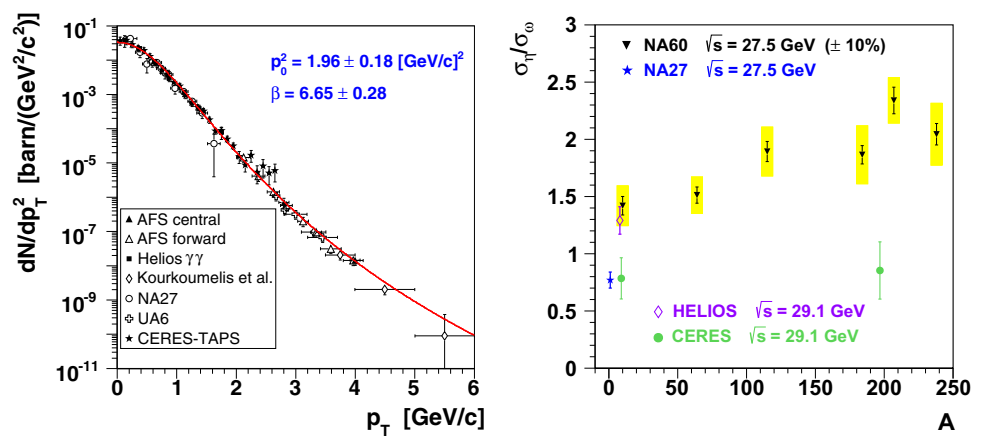
the $\sigma_\phi/\sigma_\omega$ ratio from Beryllium to Uranium, as to be expected from the difference between the p_T-integrated α_ω and α_ϕ coefficients, see Sect. 6.1. The $\sigma_\phi/\sigma_\omega$ ratio in p–p collisions can be derived from the data of the NA27 [7], NA49 [11,27] and NA61/SHINE [28] experiments. The corresponding values are also reported in Fig. 6. Given the low atomic number of the Be nucleus (with p–Be often historically taken as a proxy of p–p collisions) one might expect the $\sigma_\phi/\sigma_\omega$ ratio to show similar values in p–Be and p–p: this scenario is, however, not favoured by the data presented in Fig. 6, which suggest instead a discontinuity in the evolution of the $\sigma_\phi/\sigma_\omega$ ratio from pp to p–A. The origin of this behaviour, should it be attributed to a genuine physical mechanism, cannot be further investigated on the basis of the currently available data.

Special care must be taken when considering the $\sigma_\eta/\sigma_\omega$ ratio. Indeed, since the η is measured in the present analysis via its Dalitz decay, and only for $p_T > 0.6$ GeV/c of the muon pair, an extrapolation of the η p_T spectrum down to zero p_T was needed, to recover the η cross section in the full phase space. This full phase space extrapolation is based on a variety of available measurements, compiled in the plot shown on the left side of Fig. 7 (see [5–7,29–33]). On these data, a fit is performed with the power-law function given by Eq. (5), providing an excellent description of the points in the whole p_T range. The $\sigma_\eta/\sigma_\omega$ ratio extrapolated to the full phase space is shown in the right panel of Fig. 7. The systematic uncertainty from the extrapolation of the η measurement to full phase space amounts to ~10 %, point-to-point fully correlated. It should be remarked that

the considered extrapolation factor does not depend on the nuclear target, and it is mainly based on measurements in elementary collisions (pp, p̄p or p–Be). As a consequence, the NA60 results for the p_T-integrated $\sigma_\eta/\sigma_\omega$ ratio are properly normalised at the p–Be point, while the trend versus A should be ascribed to the nuclear dependence of the ratio in the range $p_T > 0.6$ GeV/c, where particles are measured, as to be expected from the difference between the α_ω and α_η coefficients in this same kinematic range, see Sect. 6.1.

The $\sigma_\eta/\sigma_\omega$ cross-section ratio was also measured by NA27 in p–p collisions at $\sqrt{s} = 27.5$ GeV [7], by HELIOS in p–Be collisions at $\sqrt{s_{NN}} = 29.1$ GeV [34] and by CERES-TAPS in p–Be and p–Au collisions at $\sqrt{s_{NN}} = 29.1$ GeV [5]. The corresponding measurements are shown in the right panel of Fig. 7 together with the NA60 results. The measurement of $\sigma_\eta/\sigma_\omega$ by the HELIOS experiment was derived from the $\sigma_\eta/(\sigma_\rho + \sigma_\omega)$ ratio measured in p–Be collisions through the detection of both dielectrons and dimuons, exploiting the capability to fully reconstruct the Dalitz decays. Neglecting possible ρ/ω interference effects, HELIOS obtained $\sigma_\eta/(\sigma_\rho + \sigma_\omega) = 0.54 \pm 0.05$ from the e^+e^- data and 0.52 ± 0.06 from the $\mu^+\mu^-$ data. These results were based on a $(1 + \cos^2\theta)$ decay angle distribution to extrapolate the ρ and ω measurements to full phase space. If HELIOS had assumed a uniform dimuon decay angle distribution for the ρ and ω mesons, as done in the present analysis, the full phase space ρ and ω cross sections would have been $\sim 20\%$ larger, resulting in a $\sigma_\eta/\sigma_\omega$ ratio around 1.28 ± 0.12, in agreement with the NA60 value. Finally, the CERES-TAPS $\sigma_\eta/\sigma_\omega$ measurements in p–Be and p–Au are based on the $\eta \to \gamma\gamma$ and $\omega \to \pi^0\gamma$ decay channels for $p_T > 0$, resulting in the two points also shown in the right panel of Fig. 7.

The comparison between the p–A results from NA60 and the p–p point from NA27 suggests a discontinuity in the evolution of the $\sigma_\eta/\sigma_\omega$ ratio from p–p to p–A, similar to what remarked for the $\sigma_\phi/\sigma_\omega$ ratio. The HELIOS measurement in p–Be collisions agrees with the NA60 data, while the p–Be measurement of CERES-TAPS looks compatible with the p–p point from NA27. At large A, the NA60 data cannot be directly compared to the CERES-TAPS point in p–Au, because of the different range of p_T covered by the two measurements in evaluating the nuclear dependence of the η cross section. The CERES-TAPS data, taken alone, are not conclusive about the nuclear dependence of the $\sigma_\eta/\sigma_\omega$ ratio, because of the only two nuclear targets available and the rather large statistical uncertainties.

8 Conclusions

In this letter we reported on a comprehensive study of low-mass dimuon production in p–A interactions at 400 GeV, ranging from p–Be to p–U, measured with the NA60 appara-

tus at the CERN SPS. The analysis of the p_T spectra for the ρ/ω and ϕ mesons has shown that the observed distributions cannot be explained by a thermal-like exponential function in the full p_T range accessed, while a good description of the whole observed spectrum is provided by the power-law parametrisation $dN/dp_T^2 \propto \left(1 + p_T^2/p_0^2\right)^{-\beta}$. The nuclear dependence of the cross sections of the η, ω and ϕ mesons has been found to be compatible with the power law $\sigma_{pA} \propto A^\alpha$, with a clear rising trend of the α parameters observed as a function of p_T. The observed, approximate hierarchy $\alpha_\eta \approx \alpha_\phi > \alpha_\omega$ could be attributed to the $s\bar{s}$ component in the quark wave function of the ϕ and η mesons, resulting in a harder production mechanism with respect to the ω meson. The measurement of the nuclear dependence of the production cross section ratios points to a moderate rising trend as a function of A of both the $\sigma_\eta/\sigma_\omega$ and $\sigma_\phi/\sigma_\omega$ – reflecting the observed difference in the α parameters of the η, ω and ϕ mesons – while the $\sigma_\rho/\sigma_\omega$ ratio has been found to be almost independent of the production target, and compatible with unity, in agreement with the available measurement in p–p.

References

1. T. Tabaru et al., Nuclear mass number dependence of inclusive production of ω and ϕ mesons in 12 GeV p–A collisions. Phys. Rev. C **74**, 025201 (2006)
2. R. Nasseripour et al., Search for medium modification of the ρ meson. Phys. Rev. Lett. **99**, 262302 (2007)
3. M.H. Wood et al., Absorption of the ω and ϕ Mesons in Nuclei. Phys. Rev. Lett. **105**, 112301 (2010)
4. R. Arnaldi et al., Precision study of the $\eta \to \mu^+\mu^-\gamma$ and $\omega \to \mu^+\mu^-\pi^0$ electromagnetic transition form-factors and of the $\rho \to \mu^+\mu^-$ line shape in NA60. Phys. Lett. B **757**, 437–444 (2016)
5. G. Agakishiev et al., Neutral meson production in p–Be and p–Au collisions at 450 GeV beam energy. Eur. Phys. J. C **4**, 249–257 (1998)
6. R. J. Veenhof, Low mass muon pair production in 450 GeV p–Be collisions. RX-1433 (AMSTERDAM)
7. M. Aguilar-Benitez et al., Inclusive particle production in 400-GeV/c p–p interactions. Z. Phys. C **50**, 405–426 (1991)
8. I. Abt et al., K^{*0} and phi meson production in proton–nucleus interactions at $\sqrt{(s)} = 41.6$ GeV. Eur. Phys. J. C **50**, 315–328 (2007)

9. R. Arnaldi et al., Evidence for the production of thermal-like muon pairs with masses above 1GeV/c^2 in 158A GeV indium–indium collisions. Eur. Phys. J. C **59**, 607–623 (2009)

10. S. Damjanovic, H. Woehri, A. De Falco, NA60 Internal Note 2005-1

11. S.V. Afanasev et al., Production of Phi mesons in p + p, p + Pb and central Pb + Pb collisions at E(beam) = 158-A-GeV. Phys. Lett. B **491**, 59–66 (2000)

12. T. Alber et al., Charged particle production in proton, deuteron, oxygen and sulphur nucleus collisions at 200-GeV per nucleon. Eur. Phys. J. C **2**, 643–659 (1998)

13. E.L. Bratkovskaya, W. Cassing, U. Mosel, Probing hadronic polarizations with dilepton anisotropies. Z. Phys. C **75**, 119–126 (1997)

14. A. Anastasi et al., Measurement of the $\phi \to \pi^0 e^+ e^-$ transition form factor with the KLOE detector (2016)

15. G.J. Gounaris, J.J. Sakurai, Finite width corrections to the vector meson dominance prediction for $\rho \to e^+ e^-$. Phys. Rev. Lett. **21**, 244–247 (1968)

16. K. Nakamura, Review of particle physics. J. Phys. G **37**, 075021 (2010)

17. J. Knoll, Transport dynamics of broad resonances. Prog. Part. Nucl. Phys. **42**, 177–186 (1999)

18. N.M. Kroll, W. Wada, Internal pair production associated with the emission of high-energy gamma rays. Phys. Rev. **98**, 1355–1359 (1955)

19. T. Sjostrand, S. Mrenna, P.Z. Skands, PYTHIA 6.4 physics and manual. JHEP **05**, 026 (2006)

20. R. Brun, F. Bruyant, M. Maire, A.C. McPherson, P. Zanarini, GEANT3 (1987)

21. F. Becattini, M. Gazdzicki, A. Keranen, J. Manninen, R. Stock, Chemical equilibrium in nucleus nucleus collisions at relativistic energies. Phys. Rev. C **69**, 024905 (2004)

22. K. Banicz et al., phi production in In–In collisions at 158-A-GeV. Eur. Phys. J. C **64**, 1–18 (2009)

23. A. Sibirtsev, H.W. Hammer, U.G. Meissner, A-dependence of ϕ meson production in p–A collisions. Eur. Phys. J. A **37**, 287–301 (2008)

24. L. Kluberg et al., Atomic number dependence of large transverse momentum hadron production by protons. Phys. Rev. Lett. **38**, 670–673 (1977)

25. R. Bailey et al., A-Dependence study of inclusive ϕ production. Z. Phys. C **22**, 125 (1984)

26. A.N. Aleev et al., A-Dependence of inclusive ϕ meson production in neutron–nucleus interactions at 30 GeV to 70 GeV. Czech. J. Phys. **42**, 11–19 (1992)

27. C. Alt et al., Inclusive production of charged pions in p+p collisions at 158-GeV/c beam momentum. Eur. Phys. J. C **45**, 343–381 (2006)

28. A. Marcinek, New baryonic and mesonic observables from NA61/SHINE. EPJ Web Conf. **182**, 02082 (2018)

29. C. Kourkoumelis et al., Inclusive η production at high p_T at the ISR. Phys. Lett. B **84**, 277 (1979)

30. T. Akesson et al., Production of π^0 and η at 11° in p–p collisions at $\sqrt{s} = 63$GeV. Z. Phys. C **18**, 5 (1983)

31. T. Akesson et al., A comparison of direct photon, π^0, and η production in p-$\bar{\text{p}}$ and p–p interactions at the CERN ISR. Phys. Lett. B **158**, 282–288 (1985)

32. T. Akesson et al., Inclusive η production at low transverse momentum in 63 GeV p–p collisions at the CERN interacting storage rings. Phys. Lett. B **178**, 447 (1986)

33. J. Antille et al., A measurement of the inclusive π^0 and η production cross sections at high p_T in p-$\bar{\text{p}}$ and p–p collisions at $\sqrt{s} = 24.3$GeV. Phys. Lett. B **194**, 568 (1987)

34. T. Akesson et al., Low mass lepton pair production in p–Be collisions at 450GeV/c. Z. Phys. C **68**, 47–64 (1995)